Asia-Pacific Journal of Science and Technology: Volume: 29. Issue: 02. Article ID.: APST-29-02-09. Research Article

APST

Asia-Pacific Journal of Science and Technology

https://www.tci-thaijo.org/index.php/APST/index

Published by the Research and Graduate Studies Division,
Khon Kaen University, Thailand

Corrosion inhibition properties and pKa calculations of some common corrosion inhibitors: Quantum chemical simulations

Parncheewa Toommakorn[1], Supphanat Anantachaisophon[1], Passapan Sanguanchua[1], Chanatip Sujsuntinukul[1], Adis Khetubol[1,*] and Stephen John Turner[2,*]

[1] Department of Physics and Astronomy, Kamnoetvidya Science Academy (KVIS), Rayong 21210, Thailand
[2] School of Information Science and Technology, Vidyasirimedhi Institute of Science and Technology (VISTEC), Rayong 21210 Thailand
[*]Corresponding author: Adis.k@kvis.ac.th, Steve.t@vistec.ac.th

Received 14 October 2022
Revised 2 March 2023
Accepted 14 March 2023

Abstract

Four organic compounds with various sizes, geometries, and reactive groups, namely hexylamine, morpholine, pyrazine carboxamide, and 11-mercaptoundecanoic acid, which have been reported experimentally for their corrosion inhibition property for both the bottom and the top metallic surfaces of the wet gas pipeline, are investigated by computational chemistry using density functional theory (DFT) simulations. Their inhibition properties are compared using several parameters such as HOMO/LUMO energies, global softness, and fraction of electrons transferred to metallic atoms. The reactive sites are studied through Fukui function. The fraction of protonated/deprotonated molecules to non-reactive molecules in water is determined by the acid dissociation constant, pKa, calculated over the thermodynamic cycle using Solvation Model Based on Density (SMD). Consideration of all these parameters suggests that pyrazine carboxamide may be the best potential candidate due to its highest reactivity and ability to donate electrons, with additional suitability for the top surface protection.

Keywords: Corrosion inhibitor, DFT, pK_a, SMD, Wet gas pipeline

1. Introduction

Energy is crucial for the development of this world, especially the energy from oil and natural gas deposits, formed from decaying plants and animals buried within layers of the earth and subjected to heat and pressure over millions of years [1]. Because there are demands for extracting oil from a deeper source, the additional pressure created by carbon dioxide (CO_2) is required in the oil and gas transportation system as the natural pressure for extracting oil and gas is insufficient. However, corrosion failures, which are mainly caused by the condensation of water with acid from the presence of CO_2, have led to numerous concerns.

Top-of-the-line corrosion (TLC) is a phenomenon occurring inside a wet gas transportation pipeline. Caused by the dissolution of corrosive gas species, e.g., carbon dioxide (CO_2) and hydrogen sulfide (H_2S), in the condensed water on the top of the pipeline, this issue poses a major operational challenge to the crude oil and gas extraction industry [2]. The water vapor from the increased pressure and heat will then condense in droplets on the surface of the pipeline, where corrosive species can be solvated, corroding the metal surface. Zhang et al. [3] proposed a mechanistic model to predict TLC, which covers the dropwise condensation process of water vapor and the chemical behavior of the dissolved gas species inside the condensed droplet leading to pipeline corrosion.

The conventional way of addressing this issue is to use corrosion inhibitors to reduce the corrosion to a minimum. TLC is a more serious concern than corrosion on other parts of the pipeline for two main reasons: the continually dissolved iron from the condensed droplet causes difficulty creating a protective layer, such as $FeCO_3$, and the conventional non-volatile inhibitor only protects the lower part of the pipeline [3]. TLC, if left untreated, can ultimately lead to pipeline failure and the release of hydrocarbon gases, which not only would result in environmental damage but also would be threatening to people living in the vicinity. Therefore, prevention against

TLC is crucial, and the continual search for and development of potential TLC corrosion inhibitors are of utmost importance [4, 5]. An alternative type of corrosion inhibitor was therefore proposed: a volatile corrosion inhibitor (VCI) – a compound that can reach the top of the pipeline.

VCIs are organic compounds, low nitrogen-based salts, and weak acids [6], which are able to release a vapor that can be attracted to the polar metal surface of the top of the pipeline and therefore delay TLC as the rest of the molecule is hydrophobic, which repels water [7]. VCIs are normally injected into the pipeline along with water and natural gas and will then be evaporated along with the liquid into the gas phase. Consequently, VCIs and vapors from the gas phase will undergo dropwise condensation and turn into the fluid droplet attaching to either the side or the top of the pipeline, which can protect the steel surface. In addition, for the volatile inhibitors proposed by Belarbi et al. [2, 8], the adsorption of anions or molecules possessing permanent dipole is considered likely as the steel surface in acid environments is positively charged.

Various VCIs work best under different conditions and hence are used under different circumstances [9, 10]. One of the most prevalent corrosion inhibitors for bottom-of-the-line corrosion (BLC) in the system of carbon steel submerged in an aqueous solution is morpholine. However, it was reported that morpholine does not work well for TLC inhibition, only reducing the acidity of the aqueous solution [8]. 11-mercaptoundecanoic acid, which is a thiol-based inhibitor, exhibits substantial inhibition efficiency against TLC via the formation of an adsorbed inhibitor film on the metal surface, as reported by Belarbi et al. [2]. Abdallah et al. [11] also investigated experimentally and discovered that pyrazine carboxamide, in an acidic media, exhibits good inhibiting action against the corrosion of aluminum.

Although the mechanism of TLC prevention by volatile inhibitor has been established, the calculation of some intrinsic parameters which constitute the TLC prevention efficiency of specific inhibitors, e.g., the local reactivity of the molecule and the energy gap, has yet to be determined quantitatively. This lack of a predictive model potentially leads to inefficient uses of volatile inhibitors under real circumstances – either too low resulting in ineffective protection against TLC, or too high resulting in the eventual loss of profits.

In addition to conducting experiments to determine which corrosion inhibitors are more suitable to use in a particular oil and gas pipeline condition, molecular simulations such as quantum chemical methods have been used to predict the effectiveness of corrosion inhibitors. Tan et al. [12] utilized quantum chemical analysis to determine the parameters of three particular compounds found in Passiflora edulia Sims leaves that indicate their efficacy as corrosion inhibitors for copper in sulfuric acid solution. Guo et al. [13] also conducted a quantum chemical calculation based on the density functional theory (DFT) and molecular dynamics (MD) simulation to verify the intrinsic adsorption mechanism of of 3,3-Dithiodipropionic acid (DDA) on steel surface as a corrosion inhibitor against sulfuric acid.

Ammouchi et al. [14] performed molecular simulations of pyrazine derivatives by using DFT to investigate their performance as corrosion inhibitors and the calculated quantum chemical parameters from the simulations showed a good correlation with the experimental results. However, pyrazine derivatives are the only type of VCIs investigated in this research. Moreover, all quantum chemical values were calculated from the non-protonated form of each inhibitor, but, in fact, most of the VCIs can be protonated, and the protonation notably affects their performance in inhibiting TLC.

In this work, a theoretical basis for the calculation of the inhibiting-efficiency-determining parameters is proposed for various VCIs – morpholine, hexylamine, 11-mercaptoundecanoic acid, and pyrazine carboxamide. The parameters include pK_a, first ionization energy, electron affinity, energy gap, electronegativity, global hardness, global softness, fraction of electrons transferred, electrodonating power, electroaccepting power, back-donation, and local reactivity. Some of the calculated values are compared with the available data obtained from the literature to verify the validity of the calculations. The calculated parameters are then used to determine the most suitable TLC inhibitor for a given system from the four compounds, to be used under actual circumstances.

2. Materials and Methods

To determine the parameters that play important roles in inhibition efficiency, geometry optimization and several quantum chemical calculation methods are used. In this study, density functional theory (DFT), the most appropriate calculation for molecules in ground states, using the ORCA program version 5.0.1 and 5.0.3 [15] is applied to obtain the optimized geometry of all studied molecules in Figure 1, including their protonated/deprotonated (charged) form. The hybrid functional B3LYP is utilized to approximate exchange correlations and geometry optimization, and def2-TZVP and def2-SVP basis sets, which are in the Ahlrichs def2 family, are used for the full optimization since they work well for DFT calculations on light main-group elements and other elements in a wide range [16]. Also, Self-consistent Field (SCF) calculations are tightly converged as it gives the most accurate results compared with the time used. In addition, D3 function (an atom-pairwise dispersion correction) is added to the optimization of charged molecules. Parallel programming with 7 cores is also used to speed up the calculations. These calculations provide us with several important parameters, including highest

occupied molecular orbital (E_{HOMO}), lowest unoccupied molecular orbital (E_{LUMO}), and partial charges, which will then be used for calculating the inhibiting-efficiency-determining parameters.

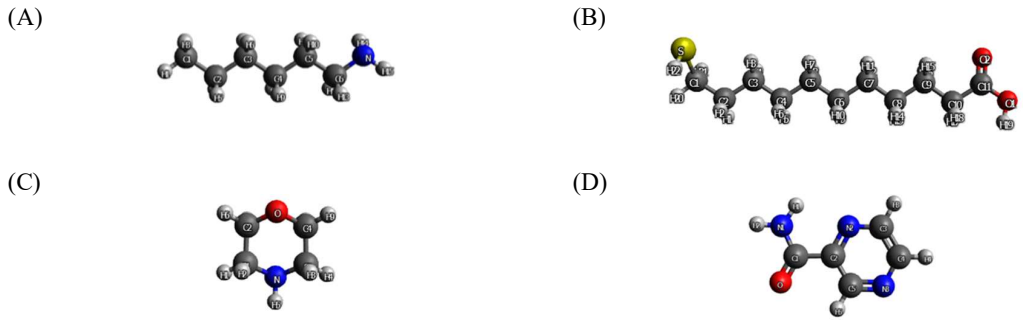

Figure 1 (A) hexylamine, (B) 11-mercaptoundecanoic acid, (C) morpholine, and (D) pyrazine carboxamide.

Parameters are calculated for both neutral and deprotonated/protonated forms, including first ionization energy (I), electron affinity (A), energy gap (ΔE), electronegativity (χ), global hardness (η), global softness (S), fraction of electrons transferred (ΔN), local reactivity, electrodonating powers (ω^-), electroaccepting powers (ω^+), and back-donation (ΔE_{back-}).

First ionization energy, electron affinity, and energy gap values are related to E_{HOMO} and E_{LUMO} as follows:

$$I = -E_{HOMO} \quad (1)$$

$$A = -E_{LUMO} \quad (2)$$

$$\Delta E = E_{LUMO} - E_{HOMO}. \quad (3)$$

The first ionization energy and the electron affinity are associated with the capacity of electron donation and acceptance of the molecule respectively. Additionally, the small amount of energy gap determines the high chemical reactivity.

Next, the obtained first ionization energy and electron affinity are used to obtain electronegativity (χ), global hardness (η), the electrodonating powers (ω^-), electroaccepting powers (ω^+), and back-donation (ΔE_{back-d}) by the following [17]:

$$\chi = \frac{I+A}{2} \quad (4)$$

$$\eta = \frac{I-A}{2} \quad (5)$$

$$\omega^- = \frac{(3I+A)^2}{16(I-A)} \quad (6)$$

$$\omega^+ = \frac{(I+3A)^2}{16(I-A)} \quad (7)$$

$$\Delta E_{back-} = -\frac{I-A}{8} \quad (8)$$

The global softness is defined as:

$$S = \frac{1}{\eta} \quad (9)$$

The global softness could be an index in the reactivity as it is inversely proportional to the stability of the molecule. The electrodonating and electroaccepting powers are global indicators introduced in [17] which refer to the amount of the small fraction of charge the molecule could donate and accept. The back-donation is a characteristic property of chemical reactivity used in estimating the charge that can be received by each molecule.

The calculated electron negativity and global hardness are used to calculate the fraction of electrons transferred, indicating the direction of charge transfer and could be an index in the inhibition efficiency of the model [16]:

$$\Delta N = \frac{\chi_{Fe} - \chi_{inh}}{2(\eta_{Fe} + \eta_{inh})} \quad (10)$$

where $\chi_{Fe} = 7$ eV and $\eta_{Fe} = 0$ by assuming that I=A for metallic bulk [17].

The dissociation reaction of basic and acidic substances can be described as follows. For basic substances:

$$A + H_2O \leftrightarrow AH^+ + OH^- \quad (11)$$

$$AH^+ + H_2O \leftrightarrow A + H_3O^+ \quad (12)$$

where the dissociation constants equal k_b and k_a respectively. From $pK_a = -\log(k_a)$ and $k_b = k_w / k_a$, the larger pK_a means the larger dissociation constant (k_b) of the basic substance. For acidic substances:

$$AH + H_2O \leftrightarrow A^- + H_3O^+ \text{ (rate} = k_a) \quad (13)$$

where the dissociation constant equals k_a. In this case, the larger pK_a means the smaller dissociation rate (k_a).

For the pK_a calculation, effects of the solvent (water) need to be considered. Therefore, a universal solvation model (SMD) is used, where the term "universal" refers to the applicability of the model to any charged or uncharged solute in any solvent or liquid for which a few key features are known. The 6-31+G(d,p) basis set is applied here as it is known as a standard basis set for any type of calculation on a wide range of molecules with the additions in polarization functions and diffuse functions. Furthermore, B3LYP and M06-2X density functional methods are used in the study to compare the accuracy in determining pKa values compared with experimental values. The calculations for protonated and non-protonated species in both vacuum and water provide us several important parameters, including final Gibbs free energy, CPCM dielectric, and SMD CDS [18].

Initially, a dissociation reaction of an acid AH can be written as:

$$AH_{(aq)} \xrightarrow{\Delta G^*_{aq}} A^-_{(aq)} + H^+_{(aq)}$$

Also, its pK_a can be calculated as:

$$pK_a = \frac{\Delta G^*_{aq}}{2.303RT} \quad (14)$$

ΔG^*_{aq} must be determined by the following equation from the thermodynamics cycle in Figure 2, from [19]:

$$\Delta G^*_{aq} = G^*_{aq}(A^-) + G^*_{aq}(H^+) - G^*_{aq}(AH) \quad (15)$$

$G^*_{aq}(H^+)$ can be obtained through this equation:

$$G^*_{aq}(H^+) = G^0_g(H^+) + \Delta G_{aq,solv}(H^+) + \Delta G^{\circ\to *} \quad (16)$$

Note that $G^0_g(H^+) = -6.29$ kcal/mol, $\Delta G_{aq,solv}(H^+) = -265.9$ kcal/mol, and $\Delta G^{\circ\to *} = RT \ln 24.46 = 1.89$ kcal/mol at RT, and $G^*_{aq}(A^-)$ and $G^*_{aq}(AH)$ can be calculated from these equations:

$$\Delta G^*_{solv}(A^-) = G^*_{aq}(A^-) + G^*_g(A^-) \quad (17)$$

$$\Delta G^*_{solv}(AH) = G^*_{aq}(AH) + G^*_g(AH) \quad (18)$$

Note that $G^*_g(A^-)$ and $G^*_g(AH)$ can be obtained by standard FREQ calculation (non-solvation) in ORCA, and ΔG^*_{solv} can be determined by the following equation:

$$\Delta G^{*}_{solv} = \Delta G_{EP} + G_{CDS} + \Delta G^{\circ \rightarrow *} \quad (19)$$

where ΔG_{EP} and G_{CDS} can be obtained from SMD solvation model in ORCA.

For the local reactivity, the partial charge on each atom can be used according to these formulas:

$$f_A^+ = q_N^A - q_{N+1}^A \quad (20)$$

$$f_A^- = q_{N-1}^A - q_N^A \quad (21)$$

where q_N^A, q_{N+1}^A, and q_{N-1}^A are the partial charge on atom A of a neutral molecule, anion, and cation (+ or – sign for positive and negative partial charge) respectively. Moreover, possible reactive sites of the molecules can also be visualized by Chemcraft program version b622b [20].

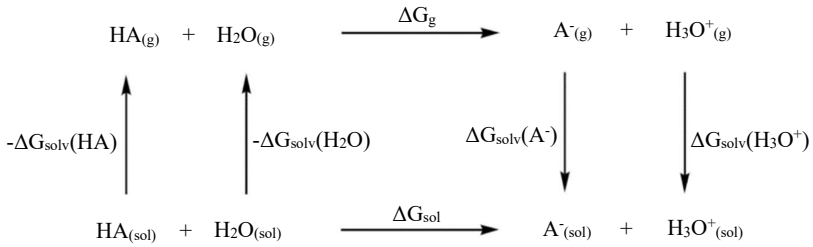

Figure 2 Thermodynamic cycle for pK_a calculation.

3. Results and discussion

3.1 Protonation

pK_a corresponds to the dissociation rate of the inhibitors in water or a weakly acidic solution of CO_2. It determines the inhibitors' ratio between the protonated/deprotonated and the neutral form. For basic molecules, the unprotonated form is the main component preventing TLC corrosion. Ions are unable to evaporate and dissolve in the droplet at the top of the line. This means the protonated inhibitors which are ions could not reach the top of the line to prevent its corrosion. Another reason the unprotonated form is more significant in this type of corrosion inhibition is that the protonated inhibitor is positively charged and is more likely to be repelled from the positively polarized iron surface, while the unprotonated inhibitors have partially negative charge resulting in attraction between the inhibitor atom and the iron surface. The inhibitor with lower pK_a would have a higher proportion of neutral atom and more molecules can evaporate to inhibit top-of-the-line corrosion. As for the acid, having a higher pK_a would yield a more neutral atom available for evaporation to prevent top-of-the-line corrosion because there is less dissociation of the neutral atom to deprotonated ions.

The pK_a values from computational calculations using different density functional methods are compared with experimental values [21] in Table 1. It can be observed that pK_a values calculated with M06-2X method are more accurate than the results calculated with B3LYP methods for all the studied molecules, except Pyrazine carboxamide where large errors are indicated.

Pyrazine carboxamide is a well-known compound in medical research but a formation of pyrazinoic acid in acidic environment is usually meant instead of its protonated form [22, 23]. Although the experimental pK_a value of the protonated pyrazine carboxamide is available in Lange [2119], there is no given indication of its protonated structure in this reference. As illustrated in Figure 1, three nitrogen sites (N1, N2, N3) can possibly be protonated: they all give negative pK_a values with a wide variation. The least negative value (-0.34) which is the closest value to the experiment (0.50) is given for the calculation with B3LYP. As previously discussed, a smaller value of pKa of a basic substance indicates less stability and less possibility of its protonated species to be formed, thus smaller k_b is implied. In other words, the large negative values in and over the range of strong acids (e.g., pK_a (HNO_3) = -1.37, pK_a (HCl) = -6.2, and pK_a (HBr) = -8.72) [21] confirm that the protonated structures of pyrazine carboxamide cannot be formed under the given environment. For this reason, the later sections only mention the neutral species of pyrazine carboxamide.

Table 1 Calculated pK_a of the studied inhibitors.

Inhibitors	Calculated $\mathbf{pK_a}$ (M06-2X)	Calculated $\mathbf{pK_a}$ (B3LYP)	Experimental $\mathbf{pK_a}$ [21]
Hexylamine (+1)	11.17	12.50	10.60
11-mercaptoundecanoic acid	4.34	5.67	4.95
Morpholine (+1)	9.11	10.20	8.49
Pyrazine carboxamide (+1)	-10.67 (N1), -6.21 (N2), -2.57 (N3)	-9.16 (N1), -3.29 (N2), -0.34 (N3)	0.50

*N1, N2 and N3 correspond to the atomic positions in Figure 1

3.2 First ionization energy, electron affinity, and energy gap

The energy gap, E_{HOMO}, E_{LUMO} of the neutral inhibitors and their protonated/deprotonated form are calculated using quantum chemistry calculation at B3LYP/def2-TZVP level. Generally, the energy gap is used to determine the inhibition efficiency of the molecule. A smaller gap means a better anti-corrosion performance of the molecule [24]. This is because, with lower energy gap, the energy needed to take away an electron in HOMO is less. So, a smaller energy gap means the molecule is more polarizable and exhibits a better electron transport capability [16], thus better reactivity and better inhibition efficiency. Among the neutral molecules, the trend of the energy gap is pyrazine carboxamide < 11-mercaptoundecanoic acid < morpholine < hexylamine, as shown in Table 2 and Figure 3(A). Pyrazine carboxamide has the lowest energy gap of 4.85 eV. The inhibitor exhibiting the second lowest energy gap, 11-mercaptoundecanoic acid, shows a significant increase from pyrazine carboxamide, with the third and fourth inhibitors showing almost the same increase from the second. The increase between the lowest and second lowest indicates a notable difference in the inhibitors' reactivity and, consequently, their performance in corrosion prevention. To summarize, the molecules which showed the most significant efficiency in corrosion prevention among the unprotonated molecules is the pyrazine carboxamide.

The protonated ions of hexylamine and morpholine show a decrease in all three values except for the energy gap of the protonated morpholine, which increases by approximately 0.3 percent. Comparing the neutral and the deprotonated form of 11-mercaptoundecanoic acid, the E_{HOMO} and E_{LUMO} of the molecule increase upon deprotonation, with the increase in the HOMO energy level more significant than the increase in the LUMO energy level, thus the energy gap decreases, increasing the molecule reactivity. Thus, using the energy gap's predictive model, the deprotonated 11-mercaptoundecanoic acid showed the best corrosion inhibition efficiency out of all the molecules.

Table 2 First ionization energy, electron affinity and ΔE of the studied inhibitors.

Inhibitors	E_{HOMO} (eV)	E_{LUMO} (eV)	ΔE (eV)	$I = -E_{HOMO}$	$A = -E_{LUMO}$
Hexylamine (H)	-6.44	0.87	7.32	6.44	-0.87
Protonated hexylamine (P-H)	-11.50	-5.14	6.36	11.50	5.14
11-mercaptoundecanoic acid (11M)	-6.44	0.05	6.49	6.44	-0.05
Deprotonated 11-mercaptoundecanoic acid (DP-11M)	-0.87	1.54	2.41	0.87	-1.54
Morpholine (M)	-6.25	0.91	7.16	6.25	-0.91
Protonated morpholine (P-M)	-12.02	-4.84	7.18	12.02	4.84
Pyrazine carboxamide (PC)	-7.03	-2.18	4.85	7.03	2.18

3.3 Electronegativity, global hardness, global softness, and fraction of electrons transferred

Softness (S) is a vital part in determining efficiency of the inhibitor as the inhibitor absorption is preferable at the region of the molecule with the highest softness value. In this case, we will consider the inhibitor as a soft base and the metal surface as a soft acid. Following that assumption, we can order the inhibitor efficiency from the softness value [16]. If the softness value increases, the efficiency increases. For the neutral molecules, the softness trend is: pyrazine carboxamide > 11-mercaptoundecanoic acid > morpholine > hexylamine, as shown in Table 3 and Figure 3(B). For the protonated molecules compared with neutral, the protonated form of hexylamine exhibits a higher softness value while that of morpholine does not change. The deprotonated form of 11-mercaptoundecanoic acid softness value increases significantly from the neutral form. Of all the molecules, the deprotonated 11-mercaptoundecanoic acid has the highest softness value and thus the best inhibition efficiency.

Table 3 Electronegativity (χ), global hardness (η), global softness (S), and fraction of electrons transferred to the metallic surface (ΔN).

Inhibitors	χ	η	S	ΔN
Hexylamine (H)	2.78	3.66	0.27	0.58
Protonated hexylamine (P-H)	8.32	3.18	0.31	-0.21
11-mercaptoundecanoic acid (11M)	3.19	3.25	0.31	0.59
Deprotonated 11-mercaptoundecanoic acid (DP-11M)	-0.33	1.21	0.83	3.04
Morpholine (M)	2.67	3.58	0.28	0.61
Protonated morpholine (P-M)	8.43	3.59	0.28	-0.20
Pyrazine carboxamide (PC)	4.60	2.43	0.41	0.49

(A)

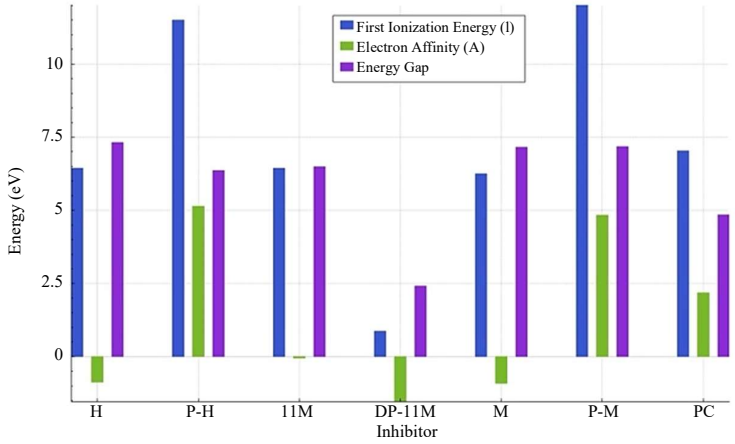

(B)

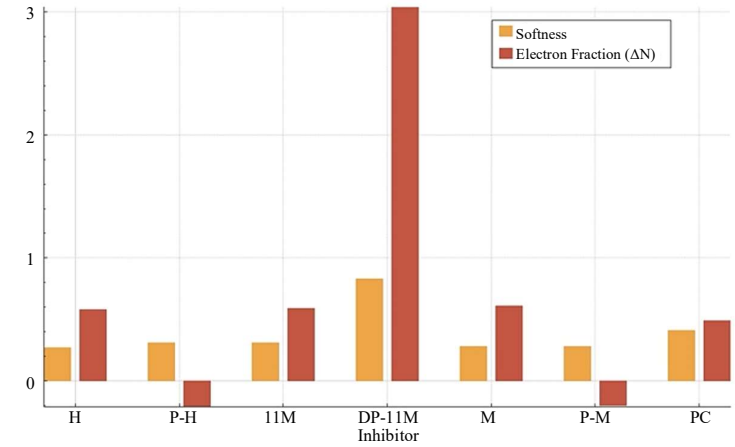

Figure 3 (A) Energy gap, ionization energy, and electron affinity of the inhibitors, (B) Global softness and electron fraction of the inhibitors.

Another crucial factor in determining the inhibition efficiency is the fraction of electrons transferred to the metallic surface (ΔN) which can determine the direction of the electron transport, positive ΔN meaning the electron flowing to the metallic surface, and vice versa for negative ΔN [16]. All the neutral molecules and the deprotonated ions exhibit a positive electron fraction which showed they acted as a nucleophile, donating electrons to the metallic pipe. The opposite is true for the two protonated ions.

3.4 Electrodonating powers, net electrophilicity index, and back-donation

In this section, parameters related to electrons transferred are determined. The first two values, ω^- and ω^+, are the global chemical reactivity indicators which indicate the capability to donate and accept a small fraction of charge respectively [25]. Thus, a high ω^- value indicates that a particular molecule has a higher capability to

donate electrons and implies that the inhibitor tends to donate electrons to the metallic surface when chemisorption occurs. From section 3.3, positive ΔN values reflect that all non-protonated inhibitors transfer their electrons to the metallic surface, so the ω^- is the focus here instead of ω^+. In addition, ΔE_{back-} is another parameter that can be used to determine the chemical reactivity of a molecule as it can be applied to predict the charge that can be received by the molecule [26]. In [25], Allal et al. observed that the higher ω^- and ΔE_{back-d}, comparing in magnitude for ΔE_{back-d}, were shown in the inhibitors with higher inhibition efficiency compared with others with the correlation coefficients of 0.9065 and 0.9486 respectively.

The calculated values of ω^-, ω^+ and ΔE_{back-d} are shown in Table 4. Among the non-pronated inhibitors, pyrazine carboxamide appears to be the best potential candidate as a corrosion inhibitor. It shows the highest values of all three parameters, followed by 11-mercaptoundecanoic acid. The values of hexylamine and morpholine are so close it is difficult to decide which one is more suitable.

Moreover, the protonated forms of inhibitors show higher values of ω^- and ω^+, but smaller values are shown in the deprotonated form of 11-mercaptoundecanoic acid compared to its neutral form. A clear trend for ΔE_{back-d} is not observed. For hexylamine and 11-mercaptoundecanoic acid, the protonated form shows a smaller value of ΔE_{back-d}. On the other hand, the protonated form of morpholine gives almost the same value compared to the neutral form. However, with the negative ΔN values for all protonated forms, higher values of ω^-, ω^+ and ΔE_{back-d} may not directly indicate the higher inhibition efficiency since the role of inhibitors as electron donors may be changed to acceptors, causing changes in inhibition mechanisms.

Table 4 Calculated electrodonating powers, electroaccepting powers, and back-donation of the studied inhibitors in (de)protonated and non-protonated form.

Inhibitors	ω^-	ω^+	ΔE_{back-d}
Hexylamine (H)	2.91	0.12	-0.91
Protonated hexylamine (P-H)	15.44	7.12	-0.80
11-mercaptoundecanoic acid (11M)	3.57	0.38	-0.81
Deprotonated 11-mercaptoundecanoic acid (DP-M11)	0.03	0.36	-0.30
Morpholine (M)	2.78	0.11	-0.89
Protonated morpholine (P-M)	14.56	6.13	-0.90
Pyrazine carboxamide (PC)	6.97	2.37	-0.61

3.5 Local reactivity

Here, active sites of molecules are determined by partial atomic charges, which show the interaction selectivity of the inhibitor molecule with the metal surface. Fukui functions for nucleophilic and electrophilic are calculated, where f_k^+ measures electron density changes when electrons are accepted, and f_k^- measures electron density changes when electrons are lost. Therefore, it is assumed the nucleophilic attack would prefer to occur at the site or region of the atom with the highest f_k^+ values. As for the electrophilic attack, it would prefer to take place in the region that has the highest f_k^- values [16]. Here, Fukui functions for nucleophilic and electrophilic attack of the non-protonated form of the studied inhibitors in vacuum are shown in Table 5. From the results ΔN, all non-protonated inhibitors tend to donate electrons, so electrophilic attack occurs to the inhibitor molecules. From the partial charge calculation, it is seen that reactive sites for the electrophilic attack mostly contains N, S, O, and may contain C in some molecules.

Table 5 Predicted reactive sites for nucleophilic and electrophilic attack with Fukui functions of the non-protonated form of studied inhibitors in vacuum.

Inhibitors	Attack	Reactive site			
Hexylamine	Nucleophilic	-			
	Electrophilic	N^{17} (0.5437)	C^1 (0.3367)		
11-mercaptoundecanoic acid	Nucleophilic	C^{11} (0.3413)			
	Electrophilic	S (0.4591)	O^2 (0.2367)	O^1 (0.2310)	
Morpholine	Nucleophilic	O (0.1046)			
	Electrophilic	N (0.2292)	C^2 (0.1985)	C^4 (0.1982)	
Pyrazine carboxamide	Nucleophilic	C^2 (0.2775)	C^1 (0.2444)		
	Electrophilic	N^1 (0.4009)	O (0.3095)	N^2 (0.2376)	N^3 (0.2341)

*See atoms' labels in Figure 1, and some examples of local reactivity visualization in Figure 4

These results are in agreement with the calculation done and visualized by Chemcraft (Figure 4). Pyrazine carboxamide again shows the most reactive site for electrophile attack by its highest f_k^- values for many atoms in the reactive region. Next tends to be 11-mercaptoundecanoic acid with lower f_k^- values, followed by hexylamine and finally morpholine. Hence, pyrazine carboxamide seems to be the best corrosion inhibitor in terms of reactivity with the metallic surface in electrophilic attack.

(A) (B)

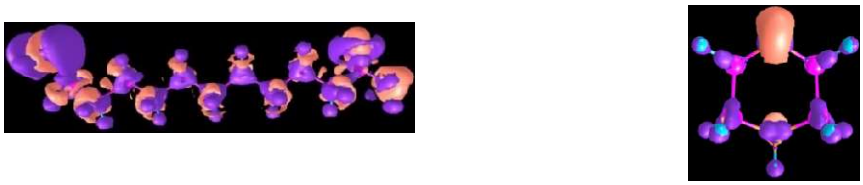

Figure 4 Local reactivity visualized by Chemcraft; (A) 11-mercaptoundecanoic acid (electrophilic attack), (B) morpholine (nucleophilic attack).

4. Conclusion

Several quantum chemistry calculations using the DFT method have been used for determining inhibition efficiency of four inhibitors with variation in sizes, geometries, and reactive groups. The parameters in this study are all related to the inhibition efficiency, which are categorized into groups, and the inhibitors have been ordered relatively for each group. For the energy gap, deprotonated 11-mercaptoundecanoic and pyrazine carboxamide show good potential as they have the lowest energy gap, which indicates the best corrosion inhibition efficiency. Moreover, for softness, deprotonated 11-mercaptoundecanoic and pyrazine carboxamide still exhibit the highest corrosion inhibition efficiency because they have the highest softness value, which means that the inhibitor absorption is preferable. Lastly, in the case of electron-transferred parameters, reflecting a capability to donate electrons, deprotonated only, pyrazine carboxamide again shows the best potential. However, hexylamine and morpholine do not show a trend that can fully determine their relative efficiency.

Considering all the calculated properties in this work, particularly its highest reactivity and ability to donate electrons, pyrazine carboxamide appears to be the most useful candidate with possibility for both top and bottom surface protection. However, to make a proper conclusion, further properties such as saturation pressure which determines the ability of a substance to undergo evaporation process must be considered. Some further simulations such as molecular dynamics simulation which provides more information on a larger-scale system should also be taken into account.

5. Acknowledgement

The authors thank Assoc. Prof. Sarana Nutanong, IST, VISTEC, for granting the students the opportunity for a research internship at IST, VISTEC and for providing us with the state-of-the-art computational resources necessary for the completion of this work, and Dr. Chatawut Chanvanichskul, PTTEP, who initiated the possibility of research within this discipline.

6. References

[1] Energy Institute. Oil and gas [Internet]. 2022 [cited 2022 Oct 4]; Available from: https://www.energyinst.org/exploring-energy/topic/oil-and-gas.

[2] Belarbi Z, Vu TN, Farelas F, Young D, Singer M, Nešić S. Thiols as volatile corrosion inhibitors for top-of-the-line corrosion. Corrosion. 2017;73(7):892-899.

[3] Zhang Z, Hinkson D, Singer M, Wang H, Nešić S. A mechanistic model of top-of-the-line corrosion. Corrosion. 2007;63(11):1051-1062.

[4] Shen M, Furman A, Kharshan R, Whited T. Development of corrosion inhibitors for prevention of top of the line corrosion (TLC) [Internet]. Texas: NACE International; 2022 [cited 2022 Oct 4]. Available from: https://www.cortecvci.com/Publications/Papers/2013-NACE-2509.pdf.

[5] Chauhan DS, Quraishi MA, Qurashi A. Recent trends in environmentally sustainable sweet corrosion inhibitors. J Mol Liq. 2021;326:115117.

[6] Abbout S. Green inhibitors to reduce the corrosion damage. In: Singh A, editor. Corrosion. London: IntechOpen; 2020. p. 1-14.

[7] Prenosil M. Volatile corrosion inhibitor coatings [Internet]. 2022 [cited 2022 Mar 22]. Available from: https://www.cortecvci.com/Publications/Papers/Nacereviewed/Pages14_17.pdf.
[8] Belarbi Z, Farelas F, Singer M, Nešić S. Role of amines in the mitigation of CO_2 top of the line corrosion. Corrosion. 2016;72(10):1300-1310.
[9] Al-Moubaraki AH, Obot IB. Top of the line corrosion: causes, mechanisms, and mitigation using corrosion inhibitors. Arab J Chem. 2021;14(5):103116.
[10] Gangopadhyay S, Mahanwar PA. Recent developments in the volatile corrosion inhibitor (VCI) coatings for metal: a review. J Coat Technol Res. 2018;15(4):789-807.
[11] Abdallah M, Sobhi M, Altass HM. Corrosion inhibition of aluminum in hydrochloric acid by pyrazinamide derivatives. J Mol Liq. 2016;223:1143-1150.
[12] Tan B, Lan W, Zhang S, Deng H, Qiang Y, Fu A, et al. Passiflora edulia sims leaves extract as renewable and degradable inhibitor for copper in sulfuric acid solution. Colloids Surf A: Physicochem Eng Asp. 2022;645:128892.
[13] Guo L, Tan J, Kaya S, Leng S, Li Q, Zhang F. Multidimensional insights into the corrosion inhibition of 3,3-dithiodipropionic acid on Q235 Steel in H_2SO_4 medium: a combined experimental and in silico investigation. J Colloid Interface Sci. 2020;570:116-124.
[14] Ammouchi N, Allal H, Belhocine Y, Bettaz S, Zouaoui E. DFT computations and molecular dynamics investigations on conformers of some pyrazinamide derivatives as corrosion inhibitors for aluminum. J Mol Liq. 2020;300:112309.
[15] Neese F. The ORCA program system. WIREs Comput Mol Sci. 2012; 2(1):73-78.
[16] Saha SK, Hens A, Murmu NC, Banerjee P. A comparative density functional theory and molecular dynamics simulation studies of the corrosion inhibitory action of two novel N-heterocyclic organic compounds along with a few others over steel surface. J Mol Liq. 2016;215:486-495.
[17] Gázquez JL, Cedillo A, Vela A. Electrodonating and electroaccepting powers. J Phys Chem A. 2007; 111(10):1966-1970.
[18] Lian P, Johnston RC, Parks JM, Smith JC. Quantum chemical calculation of pKas of environmentally relevant functional groups: carboxylic acids, amines, and thiols in aqueous solution. J Phy Chem A. 2018; 122(17):4366-4374.
[19] Pliego JR. Thermodynamic cycles and the calculation of pKa. Chem Phys Lett. 2003;367(1-2):145-149.
[20] Chemcraft. Graphical program for visualization of quantum chemistry computations [Internet]. 2021 [cited 2022 Oct 4]. Available from: http://www.chemcraftprog.com/.
[21] Dean JA. Lange's handbook of chemistry. London: Mcgraw-Hill; 1998.
[22] Zhang Y, Mitchison D. The curious characteristics of pyrazinamide: a review. Int J Tuberc Lung Dis. 2003;7(1):6-21.
[23] den Hertog AL, Menting S, Pfeltz R, Warns M, Siddiqi SH, Anthony RM. Pyrazinamide is active against mycobacterium tuberculosis cultures at neutral pH and low temperature. Antimicrob Agents Chemother. 2016;60(8):4956-4960.
[24] Chen X, Chen Y, Cui J, Li Y, Liang Y, Cao G. Molecular dynamics simulation and DFT calculation of "green" scale and corrosion inhibitor. Comput Mater Sci. 2021;188:110229.
[25] Allal H, Belhocine Y, Zouaoui E. Computational study of some thiophene derivatives as aluminium corrosion inhibitors. J Mol Liq. 2018;265:668-678.
[26] Gómez B, Likhanova NV, Domínguez-Aguilar MA, Martínez-Palou R, Vela A, Gázquez JL. Quantum chemical study of the inhibitive properties of 2-pyridyl-azoles. J Phys Chem B. 2006;110(18):8928-8934.